PAPER

Operando micro-spectroscopy on ZSM-5 containing extrudates during the oligomerization of 1-hexene†

Suzanna P. Verkleij,[a] Gareth T. Whiting, (iD) *[a] Sonia Parres Esclapez,[b] Machteld M. Mertens,[b] Anton-Jan Bons,[b] Martijn Burgers[b] and Bert M. Weckhuysen (iD) *[a]

The influence of the binder material in an industrial-type catalyst material is often neglected, although the addition of a binder can cause a significant change in the performance of the catalyst. It is difficult to visualize the effects of the different components in these multi-complex materials, and therefore, high spatiotemporal resolution techniques need to be employed. In this work, two complementary micro-spectroscopic techniques; *operando* UV-vis diffuse reflectance micro-spectroscopy (coupled to on-line mass spectrometry), and *in situ* confocal fluorescence microscopy were used to investigate the 1-hexene oligomerization reaction. The reaction was performed on both Al_2O_3- and SiO_2-bound ZSM-5-containing extrudates at 250 °C and 300 °C. By employing *operando* UV-vis micro-spectroscopy, coupled with on-line mass spectrometry, Al_2O_3-bound catalysts were found to form larger reaction products, as well as more and larger hydrocarbon deposits, compared to the SiO_2-bound catalysts. Furthermore, the extrudate containing Al_2O_3 deactivated slower than the extrudate containing SiO_2 binder. Time-resolved chemical maps of the location of the reaction products were visualized using *in situ* confocal fluorescence microscopy. The maps show that, after reaction, the zeolite crystals contain different coke species than the Al_2O_3 binder.

Introduction

ZSM-5-based catalysts are used in many industrial processes worldwide, such as crude-oil refining[1,2] and methanol to olefin (MTO) conversion.[3] Zeolite ZSM-5 is often dispersed in a binder or matrix to form millimeter-sized catalyst bodies, for example extrudates.[4] These catalyst bodies are used in industrial reactors for their superior mechanical, chemical and thermal stability, whilst achieving high catalytic activity and selectivity. Moreover, they are easier to handle and to recover than powders. For the technical body, to achieve the required properties, different materials can be used to form a complex ensemble. The active phase (*e.g.* a zeolite) can be dispersed in a binder (*e.g.* amorphous alumina or silica) for mechanical strength and in some cases, a filler (*e.g.* kaolin) is used.[5]

Although a lot of academic research has been reported on pure zeolite powder, the effect of shaping the zeolite catalyst with a binder has barely been investigated in the academic world. Considering the great use of extrudates in industrial reactors, it is vital to investigate the shaped catalyst in more detail using advanced characterization techniques. From the limited literature, it has become clear that the binder can have a large effect (beneficial or detrimental) on the catalytic activity.[5,6] Recently, Michels *et al.*[7] investigated the influence of different binders on the methanol to hydrocarbon reaction. By comparing the products and the lifetime of different binder-bound extrudates, they showed that an attapulgite binder promotes the lifetime of the catalyst as well as the selectivity towards light olefins. This was attributed to the partial ion exchange of mobile Mg species from the binder with the zeolite. Whiting *et al.*[8] showed that the selectivity during thiophene oligomerization on zeolite ZSM-5-based extrudates is dependent on the use of either a SiO_2 or Al_2O_3 binder. The zeolite ZSM-5 bound with Al_2O_3 favored a ring opening mechanism, forming thiol-like species. These examples illustrate the large influence of the binder material on the reactivity of zeolite-based catalysts. Therefore, a better understanding of these complex interactions between the

[a] *Inorganic Chemistry and Catalysis, Debye Institute for Nanomaterials Science, Utrecht University, Universiteitsweg 99, 3584 CG Utrecht, The Netherlands. E-mail: g.t.whiting@uu.nl, b.m.weckhuysen@uu.nl*
[b] *ExxonMobil Chemical Europe, Inc., European Technology Centre, Hermeslaan 2, 1831 Machelen, Belgium*
† Electronic supplementary information (ESI) available. See DOI: 10.1039/c7cy02460f

This journal is © The Royal Society of Chemistry 2018

Catal. Sci. Technol., 2018, **8**, 2175–2185 | 2175

Paper

different components in a technical catalyst body, including extrudates, is vital. This will provide further knowledge to improve the design of the technical body and in turn, enhance its process efficiency.

A difficulty in studying these catalyst bodies is the large difference in dimensions between the mm-sized extrudates and the nm/μm-sized zeolite crystals incorporated within. In recent years, non-invasive spatiotemporal characterization techniques have been developed to investigate mm-sized extrudates.[5,9] Advancements have been made in non-invasive spatiotemporal characterization techniques to visualize μm-sized FCC catalyst particles and mm-sized catalyst bodies. Examples of these techniques are UV-vis diffuse reflectance micro-spectroscopy and confocal fluorescence microscopy (CFM),[10] focused-ion-beam scanning electron microscopy (FIB-SEM),[11] X-ray tomography,[12] X-ray diffraction computed tomography (XRD-CT)[13] and NanoSIMS.[14] The combination of UV-vis micro-spectroscopy and confocal fluorescence microscopy was used to study zeolite-based extrudates.[8,15,16] However, these techniques have mainly been used to study extrudates during staining probe reactions.

In this work, we show that *operando* UV-vis diffuse reflectance micro-spectroscopy combined with on-line mass spectrometry and *in situ* confocal fluorescence microscopy, are useful tools to study catalyst extrudates during an industrially relevant reaction. The oligomerization of 1-hexene is important for the production of higher molecular weight hydrocarbons, which are used for example in lubricants.[17] Previously, it has been shown that for the 1-hexene oligomerization reaction, the product selectivity and deactivation of the catalyst depends on *e.g.* the reaction conditions (particularly reaction temperature), the catalyst used and the catalyst acidity.[18–23] The product formation for reaction temperatures between 200 °C to 450 °C have been reported previously for zeolite ZSM-5. It was found that at 200 °C, isomerization and oligomerization are the main reactions and deactivation occurs due to the formation of long oligomers that block the pores of the zeolite.[19,24] However, above 300 °C cracking of 1-hexene becomes significant and poly-aromatics are formed that block the pores and cause deactivation of the zeolite.[25–28]

Here, the 1-hexene oligomerization reaction was performed at two different temperatures (*i.e.* 250 °C and 300 °C) on mm-sized zeolite ZSM-5-containing extrudates with two different binders, namely SiO_2 and Al_2O_3. By combining *operando* UV-vis diffuse reflectance micro-spectroscopy and on-line mass spectrometry, we find that the binder choice directly influences the product formation and deactivation behavior. Furthermore, the location of the different species formed within the catalyst bodies, is also influenced by the binder choice and can be directly visualized with (*in situ*) confocal fluorescence microscopy.

Experimental

Extrudates with two different binders, namely Al_2O_3 and SiO_2, were prepared according to patent US6039864.[29] Zeolite

H-ZSM-5 crystals with a Si/Al ratio of 32 and an average crystal size of 3 μm were used to make SiO_2-bound and Al_2O_3-bound extrudates. To prepare the extrudates, the zeolite ZSM-5 crystals were mixed with H_2O, extrusion aid and binder. For the SiO_2-bound extrudates, SiO_2 gel (Aerosil 300) and silica sol (NALCOAG 1034A) were used as binder and, for the Al_2O_3-bound extrudates, pseudoboehmite alumina (Versal 300) was used as binder. The prepared mixture was extruded into 1 mm extrudates and dried overnight at 130 °C. Subsequently, the extrudates were calcined at 500 °C for 18 h. Ion-exchange was performed by suspending the extrudates in a 1 M ammonium nitrate solution for 4 h, followed by washing and drying and a final calcination at 500 °C for 18 h. The extrudates contained 20 wt% H-ZSM-5 and 80 wt% binder. A low amount of zeolite H-ZSM-5 was chosen, in order to observe the effects of the binder more clearly. Besides these samples, reference extrudates containing only the binder or H-ZSM-5 powder were used. The samples are named as follows: *A*:*B* binder, in which "*A*" corresponds to the wt% H-ZSM-5 content and "*B*" corresponds to the wt% binder. For example, 20:80 SiO_2 is a 80 wt% SiO_2-bound extrudate containing 20 wt% H-ZSM-5 crystals.

The samples were characterized with Ar physisorption, NH_3 temperature programmed desorption (TPD) and scanning electron microscopy (SEM). Before Ar physisorption, the extrudates were dried under vacuum at 300 °C overnight. All samples were measured with a Micromeritics TriStar 3000 at 77 K. The surface area was calculated with the Brunauer–Emmett–Teller (BET) method and the *t*-plot method was used to determine the pore volume. The acidity of the samples was measured with NH_3 TPD on a Mettler Toledo TGA/SDTA 851. All samples were first dried at 550 °C under He flow with a heating rate of 10 °C min^{-1} for 15 min. Subsequently, the samples were exposed to 12 pulses of 10% NH_3 in He at 100 °C. By applying a temperature ramp to 550 °C with 5 °C min^{-1} under He flow, desorption data have been collected. The amount of desorbed ammonia was monitored with a thermal conductivity detector (TCD). SEM was the last technique employed here to characterize the extrudates. A whole extrudate was attached to a SEM stub and coated with Pd/Pt in a Cressington 208HR sputter coater. The surface of the extrudate was imaged on a JEOL JSM-6340F field emission gun scanning electron microscope (FEG-SEM) operated at 5 kV using secondary electrons.

The 1-hexene oligomerization reaction was performed in an *in situ* cell (Linkam Scientific Instruments, TS1500V) equipped with a temperature controller (Linkam Scientific Instruments TMS 94 and PSU unit). 60 mg of the extrudates were placed on the heating element and, before reaction, the extrudates were calcined at 500 °C with a flow of 10 ml min^{-1} O_2 and 10 ml min^{-1} N_2. The oligomerization of 1-hexene was performed at 250 °C and 300 °C. 1-Hexene was added to a bubbler and cooled in an ice bath for 1 h before reaction to ensure reproducibility. N_2 with a flow of 20 ml min^{-1} was bubbled through the cooled 1-hexene and the products formed during the reaction were followed using an on-line

2176 | *Catal. Sci. Technol.*, 2018, **8**, 2175–2185

This journal is © The Royal Society of Chemistry 2018

mass spectrometer. The deactivation of the zeolite-based extrudates was investigated using a combination of *operando* UV-vis diffuse reflectance micro-spectroscopy and (*in situ*) confocal fluorescence microscopy.

The reaction products, that were able to leave the catalyst extrudate, were followed using a Pfeiffer Omnistar GSD 320 O3C mass spectrometer. The reaction products were analyzed with 200 ms amu^{-1} in the range of 0–200 amu. The plotted line gives the moving average of the data points. The mass spectrometer was directly coupled to the *in situ* cell and the lines between the *in situ* cell and the mass spectrometer were heated to 150 °C. *Operando* UV-vis diffuse reflectance micro-spectroscopy was performed in reflectance mode using a CRAIC 20/30 PVTM micro-spectrophotometer equipped with a 15 × 0.28 NA reflective lens. The sample was illuminated with a 30 W halogen lamp. The UV-vis diffuse reflectance spectra were collected from a spot on top of the extrudate external surface of approximately 82 × 82 μm and the spectra were recorded every 10 s for 1 h.

After reaction the sample was cooled down and measured *ex situ* with a Nikon Eclipse 90i confocal fluorescence microscope instrument equipped with a 100 × 0.73 NA dry objective. Excitation light was provided by focusing four specific laser lines; 404 nm, 488 nm, 561 nm and 642 nm on the desired sample. The emission was detected with an A1-DU4 4 detector unit and the detection ranges used were: 425–475 nm, 500–550 nm, 570–620 nm and 662–737 nm for the 404 nm, 488 nm, 561 nm and 642 nm lasers, respectively. For each extrudate, confocal fluorescence microscopy images are recorded at several different locations throughout different extrudates. The images presented in this article are representative for the observations of the extrudates. For *in situ* confocal fluorescence microscopy, the sample was reacted in the same cell as for the *operando* UV-vis diffuse reflectance micro-spectroscopy (Linkam Scientific Instruments, TS1500V). During reaction, 2-D images were taken every 30 s with the same lasers and detector.

The amount of hydrocarbon deposits inside the extrudate was characterized using thermogravimetric analysis (TGA) on a PerkinElmer pyris 1 TGA instrument. The samples were heated to 700 °C with 5 °C min^{-1} under 10 ml min^{-1} O$_2$, while the weight was measured.

Results and discussion

1. Physicochemical characterization of the catalyst materials

The external surfaces of the cylindrical 1 mm-sized extrudates under study were imaged with SEM and the images are displayed in Fig. S1 in the ESI.† The SEM images of the extrudates show that the zeolites are almost completely embedded in the extrudate and covered with the binder. SEM–EDX confirms that the zeolites (Si as marker) are homogeneously distributed throughout the Al$_2$O$_3$ binder in the 20 : 80 Al$_2$O$_3$ extrudate cross-section (Fig. S2†). This is the case for all the extrudates, whatever the binder, and shows that there is a good comparison between the different extrudates.

Pore volume and acidity of the different samples used in this study were investigated using Ar physisorption and NH$_3$ TPD, respectively. Ar physisorption in Table 1 shows that compared to the pure zeolite ZSM-5 powder, the BET surface area decreases with increasing binder content, due to the dilution of the zeolite in the sample (*i.e.*, the surface area of 20 : 80 SiO$_2$, 213 m^2 g^{-1}, is lower than that of ZSM-5 powder, 404 m^2 g^{-1}). In contrast, the total pore volume increases with increasing binder content, due to the larger pore volume present in the binder. Comparing the binder-bound extrudates, the pore volume of 20 : 80 Al$_2$O$_3$ (0.50 cm^3 g^{-1}) is higher than the pore volume of 20 : 80 SiO$_2$ (0.30 cm^3 g^{-1}). The predicted pore volumes are calculated using the ratio of pure components and are in good agreement with the experimental data, although slightly higher than expected for the Al$_2$O$_3$-bound extrudate.

The NH$_3$ TPD results (Table 1) show that the 20 : 80 Al$_2$O$_3$ extrudate contains more acid sites (0.45 mmol g^{-1} NH$_3$) than the 20 : 80 SiO$_2$ extrudate (0.12 mmol g^{-1} NH$_3$) due to the additional acid sites present in the Al$_2$O$_3$ binder (and possible creation of additional acid sites between the two components due to Si or Al migration). As expected, the SiO$_2$ binder shows no acid sites. Fig. S3† shows the NH$_3$ TPD curves. The 20 : 80 SiO$_2$ extrudate shows a similar profile as the ZSM-5 powder, showing that the SiO$_2$ binder has no influence on the acidity of the sample. For the 20 : 80 Al$_2$O$_3$ extrudate, an extra broad intermediate peak around 300 °C is present, attributed to the acid sites of the Al$_2$O$_3$ binder.

2. Catalytic performance in the oligomerization of 1-hexene at 250 °C

The extrudates were reacted with 1-hexene at 250 °C and their deactivation was followed using *operando* UV-vis diffuse reflectance micro-spectroscopy. At this reaction temperature, deactivation occurs due to the formation of long oligomers that block the acid sites.[19,23,24] The (charged) hydrocarbon species formed are known to absorb light due to their n–π^* and/or π–π^* transitions, giving rise to the formation of specific absorption bands in the UV-vis region of the spectrum. Due to the formation of a large variety of hydrocarbon species on the inside and surface of the extrudate, the absorption bands can only be assigned to a certain class of hydrocarbon species.

During 1-hexene oligomerization on both the 20 : 80 SiO$_2$ and 20 : 80 Al$_2$O$_3$ samples, several different absorption bands are formed, as shown in Fig. 1. In the first 5 min (spectra in black), absorption bands are starting to form at 32 000 cm^{-1} (310 nm) and in the region between 27 000–25 000 cm^{-1} (370–390 nm). Previous studies[30,31] have shown that these absorption bands can be assigned to charged alkylated alkenes with one or two double bonds, the mono-enyl (32 000 cm^{-1}) and di-enyl (27 000 cm^{-1}) carbenium ions. After 5 min, an absorption band at 23 000 cm^{-1} (430 nm) is formed, which can be assigned to tri-enyl carbenium ions. These absorption bands show the formation of reaction intermediates. There is no

This journal is © The Royal Society of Chemistry 2018

Catal. Sci. Technol., 2018, **8**, 2175–2185 | **2177**

Table 1 BET surface area and pore volume of the zeolite-based extrudate materials under investigation, measured with Ar physisorption. The table shows the quantity of NH$_3$ per g, measured with NH$_3$ TPD. The last two columns show the weight loss measured with TGA after reaction with 1-hexene at 250 °C or 300 °C for 1 h

	ZSM-5 : binder (wt%)	Binder	BET surface area (m^2 g^{-1})	Pore volume (cm^3 g^{-1})	NH$_3$ TPD (mmol g^{-1})	wt% residue at 250 °C	wt% residue at 300 °C
H-ZSM-5	100 : 0	—	422	0.18	0.47	11.2	9.6
SiO$_2$	0 : 100	SiO$_2$	174	0.30	0.02	1.0	1.0
20 : 80 SiO$_2$	20 : 80	SiO$_2$	209 (224)^a	0.30 (0.28)^a	0.12	3.1	3.7
Al$_2$O$_3$	0 : 100	Al$_2$O$_3$	214	0.46	0.45	9.0	8.0
20 : 80 Al$_2$O$_3$	20 : 80	Al$_2$O$_3$	245 (252)	0.50 (0.40)	0.45	11.9	8.6

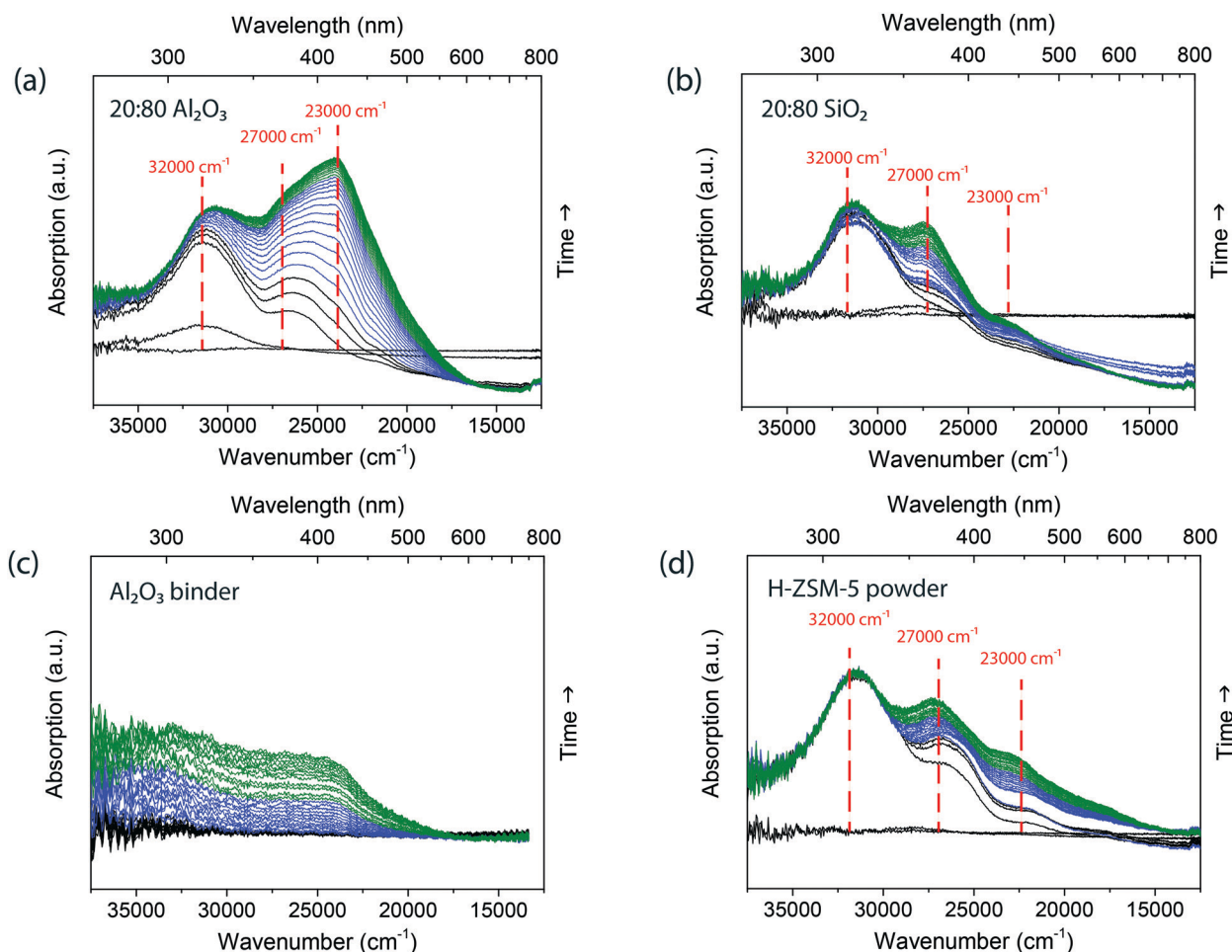^{a} Predicted BET surface areas and pore volumes calculated with the ratio of pure components.

Fig. 1 Time-resolved *operando* UV-vis diffuse reflectance spectra during the oligomerization reaction with 1-hexene at 250 °C, over (a) 20 : 80 Al$_2$O$_3$, (b) 20 : 80 SiO$_2$, (c) Al$_2$O$_3$ binder and (d) H-ZSM-5 powder for 1 h. The black spectra are taken the first 5 min, for the next 25 min the spectra are shown in blue and the last 30 min are green.

absorption band formed above 20 000 cm^{-1} (500 nm), as no large poly-aromatic coke molecules are formed. The *operando* UV-vis diffuse reflectance spectra of the two extrudates show similar band positions. However, the absorption of the band at 23 000 cm^{-1} (430 nm) is substantially higher in intensity compared to the absorption band at 32 000 cm^{-1} (310 nm) for the extrudate with Al$_2$O$_3$ binder, indicating that there is a higher concentration of larger conjugated species formed.

To distinguish between the contribution of the binder and the H-ZSM-5 crystals, each component was measured individually and the *operando* UV-vis diffuse reflectance spectra are shown in Fig. 1. The UV-vis spectra of the H-ZSM-5 powder (Fig. 1d) have similar absorption bands as the UV-vis spectra of the extrudates at 32 000 cm^{-1} (310 nm), 27 000 cm^{-1} (370 nm), 23 000 cm^{-1} (430 nm). Furthermore, the absorption bands display the same ratio as the 20 : 80 SiO$_2$ extrudates.

2178 | *Catal. Sci. Technol.*, 2018, **8**, 2175–2185

This journal is © The Royal Society of Chemistry 2018

This suggests that the SiO$_2$ binder has no significant influence on the reaction and that the extrudate with SiO$_2$ binder forms the same species as pure zeolite H-ZSM-5. Indeed, the pure SiO$_2$ binder, as presented in Fig. S4,† shows no formation of conjugated oligomers. For the Al$_2$O$_3$ binder, the *operando* UV-vis diffuse reflectance spectra, presented in Fig. 1c, show the formation of broad absorption bands in the 35 000–23 000 cm^{-1} region due to the formation of carbenium ions. However, clear bands cannot be distinguished in the UV-vis spectra. This observation is in line with the NH$_3$ TPD data of Table 1, showing that the Al$_2$O$_3$ binder has acid sites, which could form these carbenium ions.

The amounts of intermediates and products left on the used samples were analyzed with thermogravimetric analysis (TGA). The percentage of residue removed is listed in Table 1 and Fig. S5† shows the weight loss at different temperatures. The 20:80 Al$_2$O$_3$ sample (11.9 wt% residue) contains more residue than 20:80 SiO$_2$ (3.1 wt% residue). This confirms the diffuse reflectance UV-vis results that showed more large conjugated species formed on the surface of the extrudate.

To correlate the UV-vis spectral analysis with the formation of the reaction products leaving the extrudates, an on-line mass spectrometer was directly coupled to the *in situ* reaction cell. Mass spectra were measured every 40 s so that the formation of products can be followed in time. At moderate temperatures, around 250 °C, oligomerization and isomerization are the main reactions. With mass spectrometry, the formation of the dimer can be followed. Fig. 2 shows the time-resolved intensity of the 98 amu and 112 amu mass peaks (attributed to the formation of the dimer dodecene) compared to the time-resolved UV-vis absorption band formations of the zeolite-based extrudates and the individual components (a typical mass spectrum after 10 min of reaction is shown in Fig. S6†). As soon as the 1-hexene is introduced, the absorption of the 32 000 cm^{-1} (310 nm) absorption band increases in intensity and the mass spectrometer shows the formation of products, indicating that the mono-enylic carbenium ions are an intermediate in the reaction. During reaction, the intensity of the mass peaks drops slowly, coupled with a corresponding increase of the 23 000 cm^{-1} (430 nm) band, showing the formation of long conjugated oligomers that block the pores and hence, cause deactivation. Comparing the mass spectra of the two extrudates shows that the peak for the 20:80 Al$_2$O$_3$ sample remains at a higher
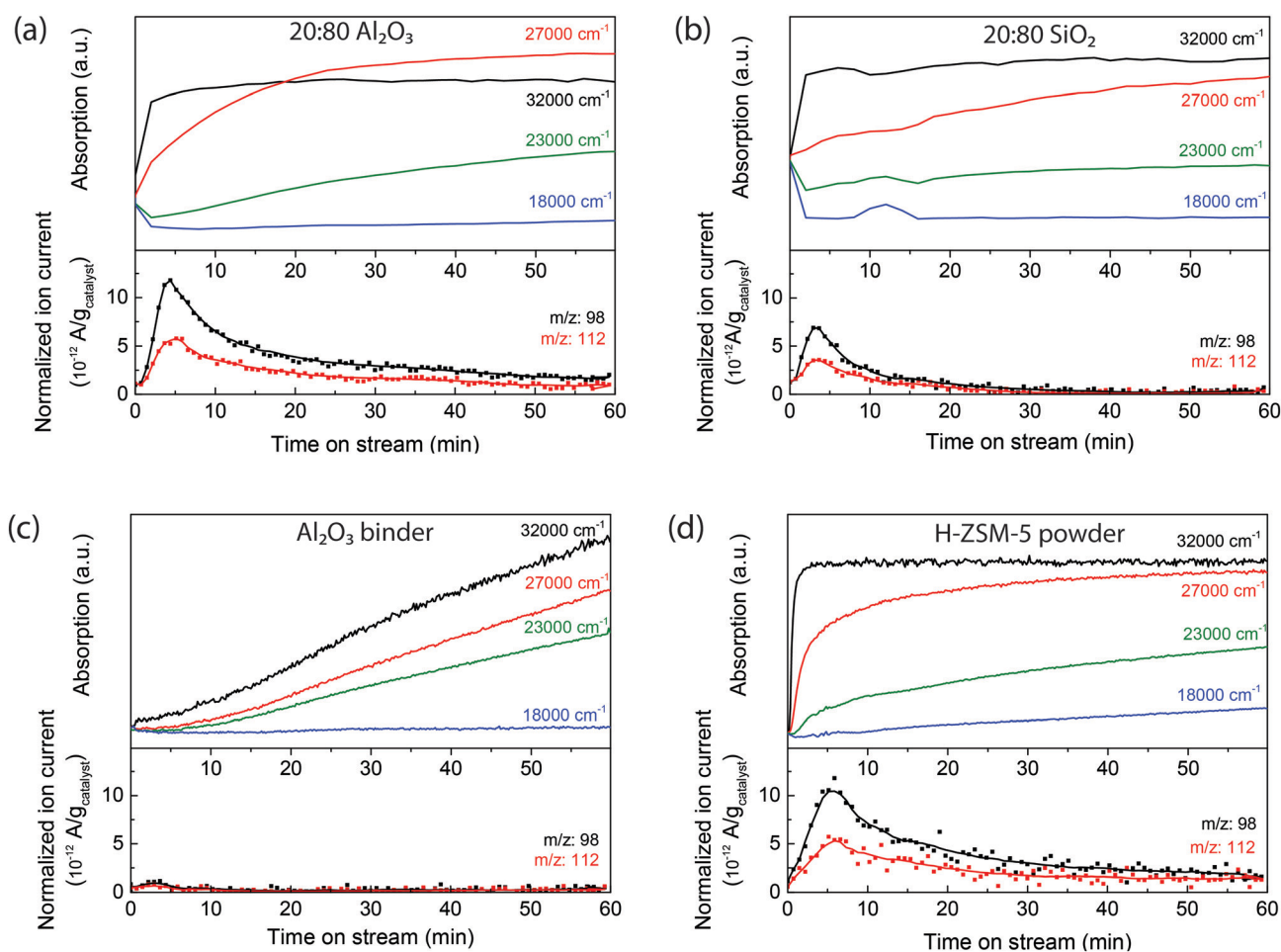

Fig. 2 Comparison of the UV-vis profiles of 32 000 cm^{-1} (black), 27 000 cm^{-1} (red), 23 000 cm^{-1} (green) and 17 000 cm^{-1} (blue) and the mass profiles of 98 amu (black) and 112 amu (blue) for (a) 20:80 Al$_2$O$_3$, (b) 20:80 SiO$_2$, (c) Al$_2$O$_3$ binder and (d) ZSM-5.

intensity over the reaction time than the 20:80 SiO$_2$ sample. A possible reason for the slower deactivation of the 20:80 Al$_2$O$_3$ extrudate could be the larger pore volume as shown by Ar physisorption in Table 1, which would enhance molecular transport compared to the SiO$_2$-bound extrudate. Furthermore, this can also be attributed to the Al$_2$O$_3$ binder, as it also participates in the reaction process. The time-resolved UV-vis absorption band of formations of the pure Al$_2$O$_3$ binder (Fig. 2c) displays the formation of charged alkenes, but the mass spectrometry does not show the formation of dimers. Therefore the Al$_2$O$_3$ binder can isomerize the 1-hexene and, in the 20:80 Al$_2$O$_3$ extrudate (Fig. 2a), these isomerized hexene molecules are easier converted into oligomers by the acid sites in the zeolites. This results in a mass peak that is more intense and prolonged. These conclusions are schematically depicted in Fig. 3a. The figure shows that 1-hexene is isomerized on the binder and subsequently oligomerized on the zeolite.

Considering the multi-scale complexity of the extrudates and the ambiguity into the role of the binders, *ex situ* confocal fluorescence microscopy can be used to visualize the location of the hydrocarbon deposits on the sample observed with *operando* UV-vis micro-spectroscopy. In a confocal fluorescence microscopy measurement, the samples were illuminated with four lasers of different wavelengths in sequence, at 404 nm, 488 nm, 561 nm and 642 nm, in order to excite molecules that absorb light in this range of wavelengths. The fluorescence light emitted was then collected *via* a pinhole, to ensure that only the in-focus light is detected. The 3-D confocal fluorescence microscope image is composed using different colors for the different fluorescence signals. With the 404 nm laser, the di-enylic species are excited and the signal is colored in blue in the image. The tri-enylic species are excited with the 488 nm laser and the signal color is green. Finally with both the 561 nm and 642 nm laser, the poly-aromatic coke species (if present) are excited and imaged in red.

Fig. 4 shows the 3-D *ex situ* confocal fluorescence images of both 20:80 Al$_2$O$_3$ and 20:80 SiO$_2$ extrudates. The green

fluorescence shows that the tri-enylic carbenium ions are mainly present inside and on the zeolite surface and there are no fluorescent molecules on the binder. Both images show no fluorescence when excited with the 561 nm and 642 nm lasers as there are no fluorescent poly-aromatic coke molecules present. This confirms the absence of absorption bands in this region of the UV-vis spectra.

Overall, the influence of the binder has been investigated during 1-hexene oligomerization at 250 °C and the results are schematically depicted in Fig. 3a. *In situ* UV-vis microspectroscopy shows that the extrudate containing Al$_2$O$_3$ binder forms more large conjugated species than the SiO$_2$-bound extrudate. Comparing the UV-vis spectra with the mass spectra shows that mainly the dimer, dodecene, is formed. Mass spectrometry confirms that more conjugated species are formed for the 20:80 Al$_2$O$_3$ extrudate than for the 20:80 SiO$_2$ extrudate, as the binder first isomerizes the 1-hexene which is subsequently easier to oligomerize in the ZSM-5 crystals. This also causes the 20:80 Al$_2$O$_3$ extrudate to deactivate slower than in the 20:80 SiO$_2$ extrudate. *Ex situ* confocal fluorescence microscopy confirms that there are no large fluorescent poly-aromatic molecules inside the zeolites and only long conjugated oligomers are present.

3. Catalytic performances in the oligomerization of 1-hexene at 300 °C

At a reaction temperature of 300 °C the isomerization and oligomerization of 1-hexene are not the only reaction pathways taking place, but cracking reactions also become important.[25–28] Kanai and Kawata[32] showed that for 1-hexene, cracking mainly occurs after oligomerization. At 300 °C, deactivation occurs not only due to the formation of long oligomers, but also by the formation of poly-aromatic species that block the acid sites.[28] The deactivation followed with *operando* UV-vis micro-spectroscopy, as presented in Fig. 5, indeed shows the formation of more poly-aromatic coke. At the start of the reaction for the 20:80 Al$_2$O$_3$ extrudate in Fig. 5a, we see absorption bands form at 34 000
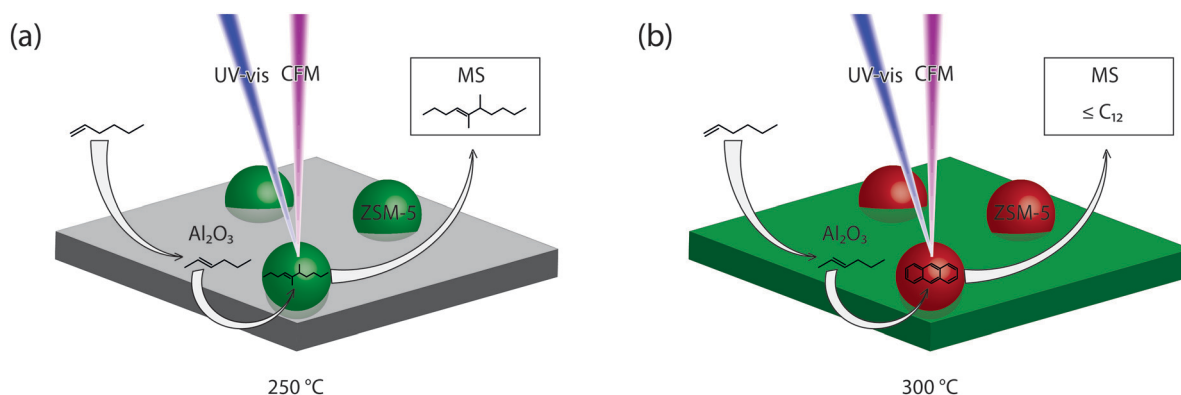

Fig. 3 Schematic overview of the reactions on the surface of the 20:80 Al$_2$O$_3$ extrudates with examples of possible molecules at (a) 250 °C and (b) 300 °C.

2180 | *Catal. Sci. Technol.*, 2018, **8**, 2175–2185

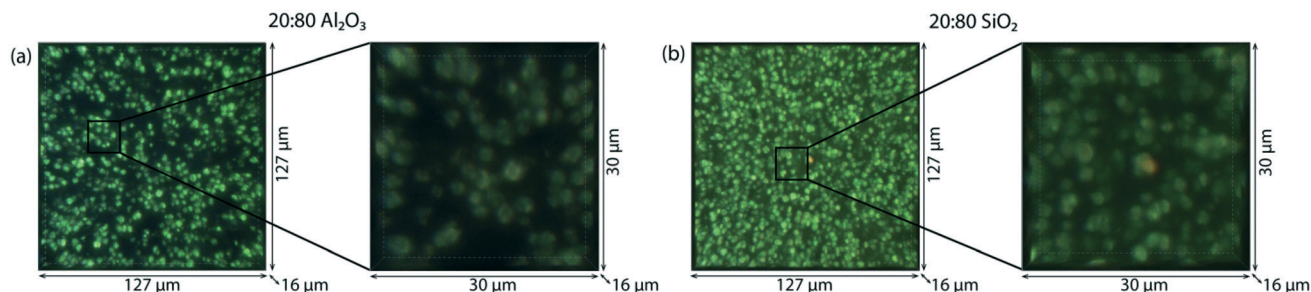This journal is © The Royal Society of Chemistry 2018

Fig. 4 *Ex situ* 3-D confocal fluorescence microscopy images taken after 1 h of 1-hexene oligomerization at 250 °C, of (a) 20 : 80 Al_2O_3, (b) 20 : 80 SiO_2. Excitation with 404 nm, 488 nm, 561 nm and 642 nm laser causes respectively the blue, green and red (both 561 and 642 nm laser) fluorescence. For all samples an enlargement of the marked area is shown on the right of the fluorescence microscopy image.
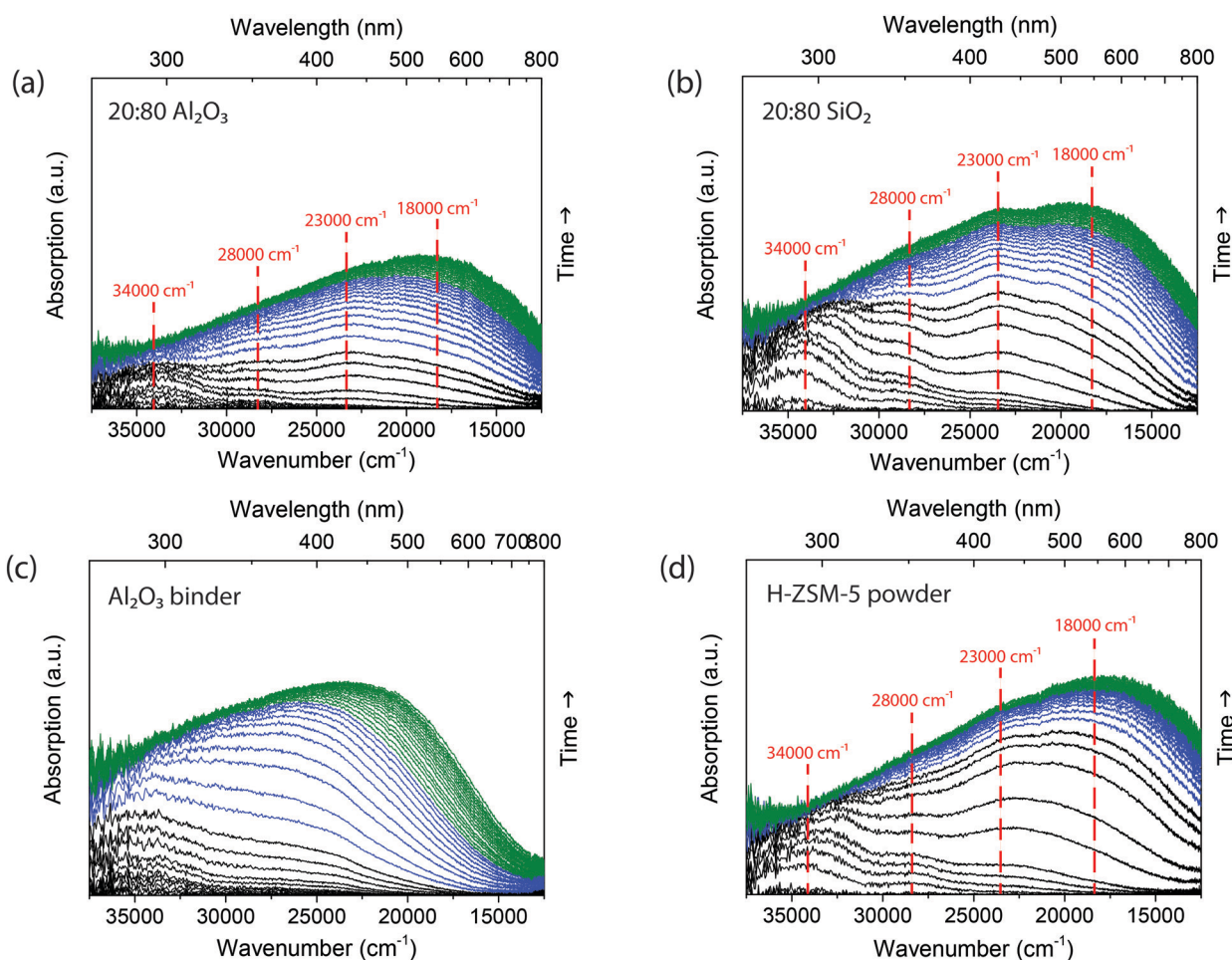

Fig. 5 Time-resolved *operando* UV-vis diffuse reflectance spectra during the oligomerization reaction with 1-hexene at 300 °C, over (a) 20 : 80 Al_2O_3, (b) 20 : 80 SiO_2, (c) Al_2O_3 binder and (d) H-ZSM-5 powder for 1 h. The black spectra are taken the first 5 min, for the next 25 min the spectra are shown in blue and the last 30 min are green.

cm^{-1} (290 nm) and a slightly shifted absorption band at 28 000 cm^{-1} (360 nm) due to the formation of both monoenylic and di-enylic carbenium ions. After 3 min (black spectra), an absorption band at 23 000 cm^{-1} (430 nm) is formed, which is assigned to both tri-enylic carbenium ions and charged alkylated aromatics.[33] At around 5 min (blue spectra) a large absorption band at 18 000 cm^{-1} (550 nm) grows in

intensity and shifts to higher wavelengths, due to the formation of poly-aromatic species.[34] This absorption band was not present in the reaction at 250 °C. Comparing the *operando* UV-vis diffuse reflectance spectra of the 20 : 80 Al_2O_3 extrudate with the 20 : 80 SiO_2 extrudate shows the formation of similar absorption bands. However, the absorption band ratio of 18 000 cm^{-1} (550 nm) to 34 000 cm^{-1} (290 nm) is

higher for the catalyst extrudate with the Al_2O_3 binder compared to the SiO_2 binder, which means that there are more large poly-aromatic coke species formed when the Al_2O_3 binder is present. The difference in coke observed with UV-vis diffuse reflectance spectroscopy was confirmed with TGA. The percentage of residue is listed in Table 1 and Fig. S7† displays the weight loss at different temperatures. The 20:80 Al_2O_3 sample (8.6 wt% coke) is confirmed to contain more coke than the 20:80 SiO_2 (3.7 wt% coke).

The UV-vis diffuse reflectance spectra of the individual components can again be compared to the spectra of the zeolite-bound extrudates. The zeolite H-ZSM-5 powder shows similar absorption bands as the extrudates and has the same ratio of absorption bands as the 20:80 SiO_2. Similar to the 250 °C reaction, the SiO_2 binder (Fig. S4†) has no effect on the absorption band ratio. For the Al_2O_3 binder, however, the *operando* UV-vis diffuse reflectance spectra in Fig. 5c display the formation of an absorption band around 34 000 cm^{-1} and a broad absorption band at 25 000 cm^{-1} (400 nm) that shifts to lower energies. This absorption band is also present in the UV-vis spectra of the 20:80 Al_2O_3

extrudate and indicates that species on the Al_2O_3 binder can grow and become more conjugated. The formation of this absorption band has a different rate for the extrudate as the combination of the two spectra, showing that the binder plays an important role in the reaction, as was also shown for the oligomerization of 1-hexene at 250 °C.

During 1-hexene oligomerization, the formation of the reaction products is studied with on-line mass spectrometry. Fig. 6 shows the intensity of the 112 amu and 105 amu mass peaks compared to the time-resolved UV-vis absorption band formations (Fig. S7† shows the mass spectra of the different samples after 10 minutes of reaction). The dimer of 1-hexene, dodecene ($C_{12}H_{24}$), has a mass peak at 168 amu, but this peak cannot be found in the mass spectrum, indicating that this is not the only product formed. Therefore, it can be concluded that the mass peak at 112 amu must be mainly a cracking product, for example octene (C_8H_{12}). This mass peak can be found in both extrudates, Al_2O_3 binder and zeolite H-ZSM-5 powder. The intensity of the 112 mass peak can be compared to the intensity of the UV-vis absorption bands during reaction. At the start of the reaction, the 112 amu
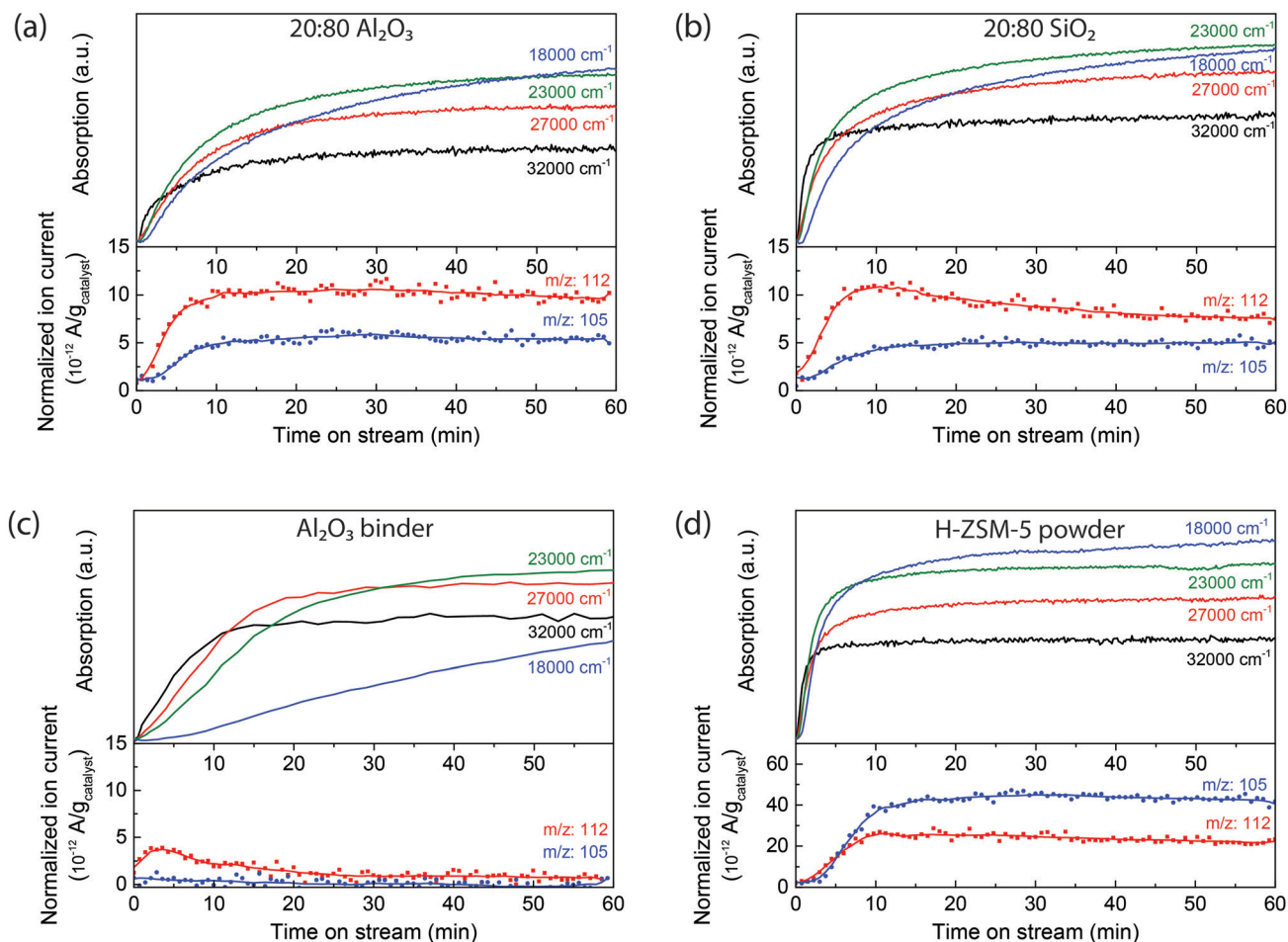

Fig. 6 Comparison of the UV-vis profiles of 32 000 cm^{-1} (black), 27 000 cm^{-1} (red), 23 000 cm^{-1} (green) and 18 000 cm^{-1} (blue) and the mass profiles of 112 amu (black) and 105 amu (red) for (a) 20:80 Al_2O_3, (b) 20:80 SiO_2, (c) Al_2O_3 binder and (d) H-ZSM-5.

2182 | *Catal. Sci. Technol.*, 2018, **8**, 2175–2185

This journal is © The Royal Society of Chemistry 2018

mass peak represents the formation of products, together with an increase of the 34 000 cm^{-1} (290 nm) absorption band, indicating that the mono-enylic carbenium ions are an intermediate in the reaction. The Al$_2$O$_3$ binder can also react with 1-hexene at this reaction temperature, and mainly isomerize the 1-hexene. The isomerized hexene molecules are easier reacted on the zeolite.

The decrease in the 112 amu mass peak is coupled with a corresponding increasing in intensity of the absorption bands at 23 000 cm^{-1} and 18 000 cm^{-1}, attributed to the formation of both long oligomers and aromatic compounds that can block the pores of the zeolite. At the same time the mass peak at 105 amu starts to increase in intensity, due to aromatic compounds that can leave the pores of the extrudate. As Fig. 6 shows, this mass peak is present for all samples containing zeolite ZSM-5 and can only be formed by the strong Brønsted acid sites. Fig. 3b schematically represents these reactions on the zeolite surface. The figure depicts the isomerization of the 1-hexene on the Al$_2$O$_3$ binder and oligomerization and cracking of the hexene on the ZSM-5. A wide variety of products can be measured with mass spectrometry and poly-aromatic species are left on the ZSM-5 crystals.

Operando UV-vis diffuse reflectance micro-spectroscopy indicates the formation of poly-aromatic species within the catalyst extrudates, which can be visualized with *ex situ* and *in situ* confocal fluorescence microscopy. To investigate if there is any visual correlation with the coke formation between the zeolite and the binder, the samples were illuminated with lasers of different wavelengths. Four different lasers were used to illuminate the sample in sequence, at 404 nm (blue), 488 nm (green), 561 nm and 642 nm (red). The *ex situ* 3-D confocal fluorescence microscopy images of the extrudates, 20:80 Al$_2$O$_3$ and 20:80 SiO$_2$, are shown in Fig. 7a and b, respectively. In both sets of microscopy images, the zeolite ZSM-5 crystals are clearly visible in orange/red, meaning that they contain species that fluoresce when excited at 561 nm and 642 nm. At both wavelengths, poly-aromatic coke species are excited and when the coke is more conjugated, the excitation wavelength becomes higher. A clear difference between the two zeolite-based extrudates is the binder. For the 20:80 SiO$_2$ extrudate, the binder is not fluorescent. However, for the extrudate with the Al$_2$O$_3$ binder, the binder shows fluorescence when excited with the 488 nm laser. Similar to the reactions at 250 °C, the tri-enylic carbenium ions are excited at this wavelength, as well as charged alkylated aromatics. This again confirms that the binder is active and that fluorescent molecules are formed on the surface of the Al$_2$O$_3$ binder.

If the components are imaged separately, the pure Al$_2$O$_3$ binder (Fig. 7c) shows fluorescence when excited with the 488 nm laser after reaction, due to the formation of tri-enylic carbenium ions or charged alkylated aromatics. This is in agreement with the *operando* UV-vis diffuse reflectance spectroscopy results where only the Al$_2$O$_3$ binder shows absorption when compared with pure SiO$_2$ binder. However, the UV-vis diffuse reflectance spectrum of the Al$_2$O$_3$ binder shows a large absorption band at 550 nm. The lack of the fluorescence signal at the excitation wavelength of 561 nm
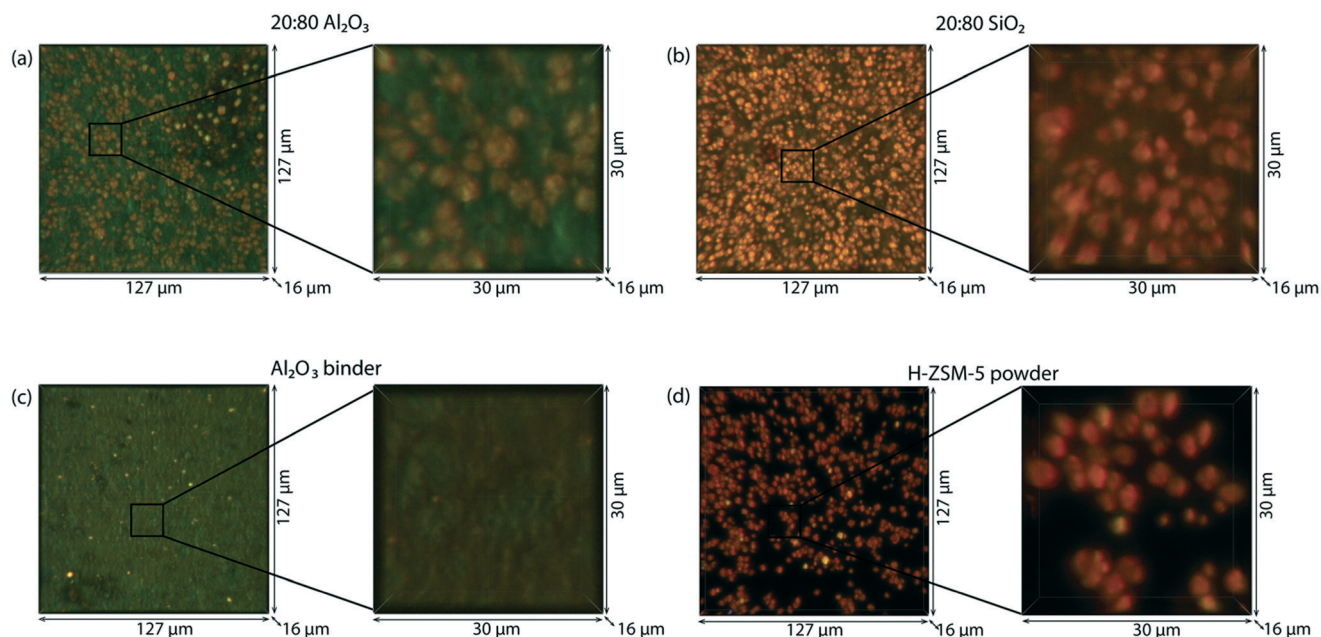

Fig. 7 *Ex situ* 3-D confocal fluorescence microscopy images taken after 1 h of 1-hexene oligomerization at 300 °C, of (a) 20:80 Al$_2$O$_3$, (b) 20:80 SiO$_2$, (c) Al$_2$O$_3$ binder and (d) H-ZSM-5 powder. Excitation with 404 nm, 488 nm, 561 nm and 642 nm lasers corresponds with blue, green and red (both 561 and 642 nm laser) fluorescence, respectively. For all samples an enlargement of the marked area is displayed to the right of the fluorescence microscopy image. The small regions of showing fluorescence upon excitation with 488 nm and 561 nm laser for the Al$_2$O$_3$ binder are impurities in the sample.

and 642 nm shows that the species formed at the extrudate surface are non-fluorescent and are probably largely conjugated olefins. For the pure zeolite H-ZSM-5 powder, the confocal fluorescence microscopy image is shown in Fig. 7d with the zeolite crystals containing species that fluoresce when excited with a wavelength of 561 nm and 642 nm. This is similar to the zeolite ZSM-5 crystals inside the catalyst extrudate bound with SiO_2 and is in line with the *operando* UV-vis diffuse reflectance spectroscopy and on-line mass-spectrometry results.

The 1-hexene oligomerization reaction can also be followed *in situ* with 2-D confocal fluorescence microscopy, as is shown in Video S1 and Video S2.† During reaction of the 20:80 SiO_2 (Video S1†) extrudate, the fluorescence with the 561 nm and 642 nm laser becomes more intense, showing the formation and growth of poly-aromatic coke molecules inside the zeolite, comparable to the UV-vis diffuse reflectance spectra. The 20:80 Al_2O_3 extrudate (Video S2†) shows similar growth of poly-aromatic coke molecules but, significantly, also shows the formation of tri-enylic carbenium ions inside the binder, again confirming the role of the Al_2O_3 binder in the reaction. The final image is similar as the *ex situ* image, showing that it is indeed possible to compare the *ex situ* confocal fluorescence microscopy images after reaction and shows the potential of this technique to visualize the location and formation of fluorescent molecules in catalyst systems.

Conclusions

Using two complementary micro-spectroscopic techniques, *operando* UV-vis diffuse reflectance micro-spectroscopy (coupled to on-line mass spectrometry), and (*in situ*) confocal fluorescence microscopy, we were able to gain more insight on the influence of the binder in extrudates during an industrially relevant reaction. Zeolite H-ZSM-5-bound extrudates with SiO_2 or Al_2O_3 binder were investigated during 1-hexene oligomerization at 250 °C and 300 °C. The employed techniques demonstrate that the performance of the extrudates during reaction is largely influenced by the binder material. By using a combination of *operando* UV-vis micro-spectroscopy with mass spectrometry, we have been able to correlate the role of the binder and the deactivation mechanisms of the catalyst extrudates. The extrudates bound with Al_2O_3 deactivate at a slower rate and form more conjugated species than the extrudates containing SiO_2. This was due to the Al_2O_3 binder reacting with 1-hexene to form molecules that are more easily transformed by the zeolite. The location of the hydrocarbon deposits was visualized with *in situ* confocal fluorescence microscopy. At 300 °C, large poly-aromatic coke molecules are situated on the zeolite for both extrudates. However, for the extrudate bound with Al_2O_3, large conjugated hydrocarbons are situated on the binder, showing, in real-time, the participation of the binder during the reaction.

Conflicts of interest

There are no conflicts to declare.

References

1 A. Corma, M. J. Díaz-Cabañas, J. Martínez-Triguero, F. Rey and J. Rius, *Nature*, 2002, **418**, 514–517.

2 W. Vermeiren and J.-P. Gilson, *Top. Catal.*, 2009, **52**, 1131–1161.

3 M. Stöcker, *Microporous Mesoporous Mater.*, 1999, **29**, 3–48.

4 P. A. Jacobs, E. M. Flanigen, J. C. Jansen and H. van Bekkum, *Introduction to Zeolite Science and Practice*, Elsevier, Amsterdam, 2001.

5 S. Mitchell, N.-L. Michels and J. Pérez-Ramírez, *Chem. Soc. Rev.*, 2013, **42**, 6094–6112.

6 J. S. J. Hargreaves and A. L. Munnoch, *Catal. Sci. Technol.*, 2013, **3**, 1165–1171.

7 N.-L. Michels, S. Mitchell and J. Pérez-Ramírez, *ACS Catal.*, 2014, **4**, 2409–2417.

8 G. T. Whiting, F. Meirer, M. M. Mertens, A.-J. Bons, B. M. Weiss, P. A. Stevens, E. de Smit and B. M. Weckhuysen, *ChemCatChem*, 2015, **7**, 1312–1321.

9 M. M. Kerssens, C. Sprung, G. T. Whiting and B. M. Weckhuysen, *Microporous Mesoporous Mater.*, 2014, **189**, 136–143.

10 J. Ruiz-Martínez, I. L. C. Buurmans, W. V. Knowles, D. Van Der Beek, J. A. Bergwerff, E. T. C. Vogt and B. M. Weckhuysen, *Appl. Catal., A*, 2012, **419–420**, 84–94.

11 L. Karwacki, D. A. M. De Winter, L. R. Aramburo, M. N. Lebbink, J. A. Post, M. R. Drury and B. M. Weckhuysen, *Angew. Chem., Int. Ed.*, 2011, **50**, 1294–1298.

12 J.-D. Grunwaldt and C. G. Schroer, *Chem. Soc. Rev.*, 2010, **39**, 4741–4753.

13 J. Ruiz-Martínez, A. M. Beale, U. Deka, M. G. O'Brien, P. D. Quinn, J. F. W. Mosselmans and B. M. Weckhuysen, *Angew. Chem.*, 2013, **125**, 6099–6103.

14 A. J. Martin, S. Mitchell, K. Kunze, K. C. Weston and J. Pérez-Ramírez, *Mater. Horiz.*, 2017, **4**, 857–861.

15 G. T. Whiting, F. Meirer, D. Valencia, M. M. Mertens, A.-J. Bons, B. M. Weiss, P. A. Stevens, E. de Smit and B. M. Weckhuysen, *Phys. Chem. Chem. Phys.*, 2014, **16**, 21531–21542.

16 P. Castaño, J. Ruiz-Martínez, E. Epelde, A. G. Gayubo and B. M. Weckhuysen, *ChemCatChem*, 2013, **5**, 2827–2831.

17 S. H. Brown, G. M. K. Mathys and P. Hamilton US7572947B2, 2009.

18 X. Li, C. Wang, S. Liu, W. Xin, Y. Wang, S. Xie and L. Xu, *J. Mol. Catal. A: Chem.*, 2011, **336**, 34–41.

2184 | *Catal. Sci. Technol.*, 2018, **8**, 2175–2185

This journal is © The Royal Society of Chemistry 2018

19 A. de Klerk, *Ind. Eng. Chem. Res.*, 2005, **44**, 3887–3893.

20 J. P. G. Pater, P. A. Jacobs and J. A. Martens, *J. Catal.*, 1999, **184**, 262–267.

21 R. Van Grieken, J. M. Escola, J. Moreno and R. Rodríguez, *Appl. Catal., A*, 2006, **305**, 176–188.

22 S. J. Choung and J. B. Butt, *Appl. Catal.*, 1990, **64**, 173–189.

23 J. P. G. Pater, P. A. Jacobs and J. A. Martens, *J. Catal.*, 1998, **179**, 477–482.

24 J. Abbot, A. Corma and B. W. Wojciechowski, *J. Catal.*, 1985, **92**, 398–408.

25 J. Abbot and B. W. Wojciechowski, *Can. J. Chem. Eng.*, 1985, **63**, 451–461.

26 Y. Li, S. Liu, Z. Zhang, S. Xie, X. Zhu and L. Xu, *Appl. Catal., A*, 2008, **338**, 100–113.

27 L. Zhang, H. Liu, X. Li, S. Xie, Y. Wang, W. Xin, S. Liu and L. Xu, *Fuel Process. Technol.*, 2010, **91**, 449–455.

28 J. R. Anderson, Y.-F. Chang and R. J. Western, *J. Catal.*, 1989, **118**, 466–482.

29 G. D. Mohr and J. P. Verduijn, US6039864A, 2000.

30 I. Kiricsi, G. Tasi, H. Förster and P. Fejes, *J. Mol. Struct.*, 1990, **218**, 369–374.

31 I. Kiricsi and H. Förster, *J. Chem. Soc., Faraday Trans. 1*, 1988, **84**, 491–499.

32 J. Kanai and N. Kawata, *J. Catal.*, 1988, **114**, 284–290.

33 K. Hemelsoet, Q. Qian, T. De Meyer, K. De Wispelaere, B. De Sterck, B. M. Weckhuysen, M. Waroquier and V. Van Speybroeck, *Chem. – Eur. J.*, 2013, **19**, 16595–16606.

34 D. Mores, J. Kornatowski, U. Olsbye and B. M. Weckhuysen, *Chem. – Eur. J.*, 2011, **17**, 2874–2884.

This journal is © The Royal Society of Chemistry 2018

Catal. Sci. Technol., 2018, **8**, 2175–2185 | **2185**